

DTP/98/98
December 1998

Penetration of the Earth by ultrahigh energy neutrinos predicted by low x QCD

J. Kwiecinski^{a,b}, A.D. Martin^b and A.M. Stasto^{a,b}

^a H. Niewodniczanski Institute of Nuclear Physics, ul. Radzikowskiego 152, Krakow, Poland

^b Department of Physics, University of Durham, Durham, DH1 3LE

Abstract

We calculate the cross sections for neutrino interactions with (isoscalar) nuclear targets in the energy domain all the way up to 10^{12} GeV. Small x QCD effects are included by using a unified BFKL/DGLAP formalism which embodies non-leading $\log 1/x$ contributions. The few free parameters which specify the input parton distributions are determined by fitting to HERA deep inelastic data. The attenuation of neutrinos transversing the Earth at different nadir angles is calculated for a variety of energy spectra for neutrinos originating from different sources (from Active Galactic Nuclei, Gamma ray bursts, top-down models), as well as for atmospheric neutrinos. For this purpose we solve the transport equation which includes regeneration due to neutral current neutrino interactions, besides attenuation.

1. Introduction

The penetration of ultrahigh energy neutrinos through the Earth, with energies E greater than 10 TeV or so, can be strongly affected by neutrino interactions with matter. This is due to the increase of neutrino cross sections with energy. At these ultrahigh energies we have significant attenuation of the neutrino fluxes on transversing through the Earth and, indeed, complete absorption for energies above about 10^8 GeV or so, depending on the nadir angle of the neutrino beam. Realistic estimates of these effects are crucial for predicting the number of neutrinos reaching the large km^3 scale detectors after penetration through the Earth. Clearly the magnitude of this ultrahigh energy neutrino flux has important implications for neutrino astronomy. For example, it is hoped that the neutrino flux coming through the Earth will point back to its Active Galactic Nuclei (AGN) origin [1]. Clearly the magnitude of the signal, and the ability of the Earth to reduce the background due to atmospheric neutrinos, are crucial in this exciting endeavour.

The inelastic interaction of neutrinos with nucleons is traditionally described by the QCD-improved parton model. In ultrahigh energy neutrino interactions we are probing a kinematical region which is not accessible in current collider experiments. To be precise the most powerful electron-proton collider HERA at the DESY laboratory in Hamburg typically probes the region $x > 10^{-4}$ for $Q^2 > 10 \text{ GeV}^2$, whereas the ultrahigh energy neutrino interactions can become sensitive to the domain $x \sim 10^{-8}$ and $Q^2 \sim M_W^2$. Here, as usual, x denotes the Bjorken scaling variable and $Q^2 = -q^2$, where q is the four momentum transfer between the leptons in the inelastic scattering of a lepton on a nucleon. The Bjorken variable x is defined as $x = Q^2/(2p \cdot q)$ where p denotes the four momentum of the nucleon.

In perturbative QCD it is expected that the gluon and sea-quark distributions, and hence also the deep inelastic scattering structure functions, should grow with the decreasing values of the parameter x . This theoretical expectation has been beautifully confirmed by the structure function measurements at HERA [2]. These measurements put important constraints on parton distributions in the small x region probed at HERA. In order to get predictions for the ultrahigh energy neutrino-nucleon cross sections one has to construct a reliable extrapolation of the structure functions to the region of very small values of x which is probed in these ultrahigh energy interactions. The existing extrapolations, which do also incorporate the constraints from the HERA data, are based entirely on leading order (LO) or next-to-leading order (NLO) DGLAP evolution [3, 4, 5]. This approximation may, however, be incomplete at low x since it ignores the important resummation of $\ln(1/x)$ BFKL-type effects [6]. In this paper we wish to incorporate the QCD expectations at low x which will take these effects into account. To be precise we shall base our calculation of the neutrino cross sections on the unified BFKL/DGLAP formalism which incorporates both the $\ln(1/x)$ resummation and the complete LO DGLAP evolution [7]. Due to the size of the NLO $\ln(1/x)$ contributions [8] one might question the reliability of this procedure. However our framework makes it possible to resum dominant non-leading $\ln(1/x)$ contributions to all orders. This has the important effect of stabilizing the non-leading contribution and turns out to give a physically and phenomenologically acceptable

suppression of the LO BFKL behaviour. In this way we should achieve the most reliable dynamically-motivated extrapolation to very low x to date, which incorporates all the relevant QCD expectations. The calculated neutrino cross sections are then used as an input in transport equation describing the propagation of the neutrinos through the Earth [9, 10]. This equation will contain both the attenuation of the neutrino flux together with its regeneration through the neutral current interaction. Similar calculation which takes into account absorption and gives prediction for the muon rates has been performed in [11].

The content of our paper is as follows. In the next Section we discuss deep inelastic lepton-nucleon scattering at low x within the unified BFKL/DGLAP framework. In Sec. 3 we collect the relevant formulas needed for calculating the neutrino cross sections and present our numerical results for these cross sections calculated within the unified BFKL/DGLAP scheme. We also confront our predictions with results of calculations based on NLO DGLAP evolution. Sec. 4 is devoted to the discussion of the transport equation and its solution for the shadowing factor due to passage of the neutrinos through the Earth. In Sec. 5 we present our results concerning the changes of the initial fluxes with nadir angle. We consider neutrino fluxes corresponding to Active Galactic Nuclei, Gamma Ray Bursts and the Top-Down models, together with atmospheric neutrino background. Finally in Sec. 6 we give our conclusions.

2. Deep inelastic scattering at low x

Ultrahigh energy neutrino-nucleon interactions probe values of Bjorken x which can be several orders of magnitude smaller than those which are accessible at the present deep inelastic ep scattering experiments at HERA. Here, as usual, $x = Q^2/2p \cdot q$ where $Q^2 \equiv -q^2$, with p denoting the nucleon 4-momentum and q being the 4-momentum transfer between the leptons in the deep-inelastic process $\ell N \rightarrow \ell' X$.

At low values of x we must consider $\log(1/x)$ effects. In ref. [7] a formalism is presented which permits an extrapolation of parton distributions to very small x . Besides the leading order (LO) $\log(1/x)$ resummation, the procedure incorporates a major part of an all-order resummation. We outline the method below. We begin with the BFKL equation [6] for the unintegrated gluon distribution $f(x, k_T^2)$, which performs the LO $\log(1/x)$ resummation. The equation has the form

$$f(x, k^2) = f^{(0)}(x, k^2) + \bar{\alpha}_S k^2 \int_x^1 \frac{dz}{z} \int \frac{dk'^2}{k'^2} \left\{ \frac{f(x/z, k'^2) - f(x/z, k^2)}{|k'^2 - k^2|} + \frac{f(x/z, k^2)}{[4k'^4 + k^4]^{\frac{1}{2}}} \right\} \quad (1)$$

where $\bar{\alpha}_S = N_c \alpha_S / \pi$ and $k = k_T, k' = k'_T$ denote the transverse momenta of the gluons, see Fig. 1. The term in the integrand containing $f(x/z, k'^2)$ corresponds to real gluon emission, whereas the terms involving $f(x/z, k^2)$ represent the virtual contributions and lead to the Reggeization of the t -channel exchanged gluons. The inhomogeneous driving term $f^{(0)}$ will be specified later.

The observable nucleon structure functions F_i are given in terms of the gluon distribution by the k_T factorization formula [15]

$$F_i(x, Q^2) = \int_x^1 \frac{dz}{z} \int \frac{dk^2}{k^2} F_i^{\text{box}}(z, k^2, Q^2) f\left(\frac{x}{z}, k^2\right), \quad (2)$$

where F_i^{box} describes the subprocess $Vg \rightarrow q\bar{q}$, see Fig. 1. Here the virtual gauge boson V may be either a γ (describing an electromagnetic deep inelastic scattering) or a W^\pm boson (describing a charged current weak interaction) or a Z boson (describing a neutral current weak interaction). The procedure (1) and (2) automatically resums all the leading $\log(1/x)$ contributions to the observable F_i .

The solution of the LO BFKL equation for fixed α_S gives a QCD or hard pomeron with intercept $\alpha(0) = 1 + \lambda$ with $\lambda = \bar{\alpha}_S 4 \ln 2$. The $\ln(1/x)$ resummation has recently been carried out [8] at next-to-leading order (NLO). It is found to give a very large $O(\alpha_S^2)$ correction to λ

$$\lambda \simeq \bar{\alpha}_S 4 \ln 2 (1 - 6\bar{\alpha}_S), \quad (3)$$

which implies that the NLO approximation is unreliable for realistic values of α_S . Rather we must use a formalism which contains an estimate of an all-order resummation. Clearly it would be desirable to identify physical effects which could be resummed to all orders and which at the same time yield a NLO value of λ that is comparable to (3). As it happens the imposition of the consistency constraint [12, 13]

$$k'^2 < k^2/z \quad (4)$$

on the real gluon emission term gives just such an effect. The variables are shown in Fig. 1. The origin of the constraint is the requirement that the virtuality of the exchanged gluon is dominated by its transverse momentum $|k'^2| \simeq k_T'^2$. For clarity we have restored the subscript T in this equation.

If condition (4) is imposed on the BFKL equation it can be still solved analytically. The result is an all-order effect, which at NLO gives the large modification

$$\lambda \simeq \bar{\alpha}_S 4 \ln 2 (1 - 4.2\bar{\alpha}_S) \quad (5)$$

of the LO value. However it is found that the all-order correction is a much milder modification, although still significant. A related result can be found in ref. [14]. We can therefore make the BFKL equation (1) for the gluon much more realistic by imposing the consistency condition (4), as well as by allowing the coupling α_S to run.

Moreover we can extend its validity to cover the full range of x . To do this we note that the BFKL equation embodies the important double leading log part of DGLAP evolution which is driven just by the singular $1/z$ part of the splitting function P_{gg} . To obtain a reliable description throughout the full x range (and not just at small x) we must include the remaining terms in P_{gg} , together with the quark to gluon transitions. We also introduce in eq. 1 the parameter k_o^2 ($k_o^2 \simeq 1 \text{ GeV}^2$) which divides the non-perturbative ($k'^2 < k_o^2$) from the perturbative ($k'^2 > k_o^2$) region. Finally we note that the contribution from the infrared region $k'^2 < k_o^2$ in (1) may be expressed [7] in terms of the integrated gluon distribution at scale k_o^2 , that is $g(x, k_o^2)$. All the above modifications of (1) are encapsulated in a unified BFKL/DGLAP equation of the form

$$\begin{aligned}
f(x, k^2) &= \tilde{f}^{(0)}(x, k^2) + \\
&+ \bar{\alpha}_S(k^2) k^2 \int_x^1 \frac{dz}{z} \int_{k_0^2} \frac{dk'^2}{k'^2} \left\{ \frac{f\left(\frac{x}{z}, k'^2\right) \Theta\left(\frac{k^2}{z} - k'^2\right) - f\left(\frac{x}{z}, k^2\right)}{|k'^2 - k^2|} + \frac{f\left(\frac{x}{z}, k^2\right)}{[4k^4 + k^4]^{\frac{1}{2}}} \right\} \quad (6) \\
&+ \bar{\alpha}_S(k^2) \int_x^1 \frac{dz}{z} \left(\frac{z}{6} P_{gg}(z) - 1 \right) \int_{k_0^2}^{k^2} \frac{dk'^2}{k'^2} f\left(\frac{x}{z}, k'^2\right) + \frac{\alpha_S(k^2)}{2\pi} \int_x^1 dz P_{gg}(z) \Sigma\left(\frac{x}{z}, k^2\right).
\end{aligned}$$

Now the driving term has the form

$$\tilde{f}^{(0)}(x, k^2) = f^{(0)}(x, k^2) + \frac{\alpha_S(k^2)}{2\pi} \int_x^1 dz P_{gg}(z) \frac{x}{z} g\left(\frac{x}{z}, k_0^2\right) \quad (7)$$

where in the perturbative domain $k^2 > k_0^2$ we may safely neglect the genuinely non-perturbative contribution $f^{(0)}(x, k^2)$ which is expected to decrease rapidly with increasing k^2 . It is important to note that (6) only involves $f(x, k^2)$ in the perturbative region $k^2 > k_0^2$. The input (7) is provided by the conventional gluon at scale k_0^2 , just as in pure DGLAP evolution.

The last term in (6) is the contribution of the singlet quark distribution to the gluon, with

$$\Sigma = \sum_q x(q + \bar{q}) = \sum_q (S_q + V_q) \quad (8)$$

where S and V denote the sea and valence quark momentum distributions. The gluon, in turn, helps to drive the sea quark distribution through the $g \rightarrow q\bar{q}$ transition. Thus equation (6) has to be solved simultaneously with an equivalent equation for $\Sigma(x, k^2)$.

Consider for the moment just the $g \rightarrow q\bar{q}$ contribution to S_q . The k_T factorization theorem gives [15]

$$S_q(x, Q^2) = \int_x^1 \frac{dz}{z} \int \frac{dk^2}{k^2} S_{\text{box}}^q(z, k^2, Q^2) f\left(\frac{x}{z}, k^2\right) \quad (9)$$

where S^{box} describes the quark box (and crossed-box) contribution shown in Fig. 1. S^{box} implicitly includes an integration over the transverse momentum κ of the exchanged quark. We have

$$\begin{aligned}
S_q^{\text{box}}(z, k^2, Q^2) &= \frac{Q^2}{4\pi^2 k^2} \int_0^1 d\beta \int d^2 \kappa' \alpha_S \left\{ [\beta^2 + (1 - \beta)^2] \left(\frac{\kappa}{D_{1q}} - \frac{\kappa - \mathbf{k}}{D_{2q}} \right)^2 \right. \\
&+ \left. [m_q^2 + 4Q^2 \beta^2 (1 - \beta)^2] \left(\frac{1}{D_{1q}} - \frac{1}{D_{2q}} \right)^2 \right\} \delta(z - z_0) \quad (10)
\end{aligned}$$

where $\kappa' = \kappa - (1 - \beta)\mathbf{k}$ and

$$\begin{aligned}
D_{1q} &= \kappa^2 + \beta(1 - \beta)Q^2 + m_q^2 \\
D_{2q} &= (\kappa - \mathbf{k})^2 + \beta(1 - \beta)Q^2 + m_q^2 \\
z_0 &= \left[1 + \frac{\kappa'^2 + m_q^2}{\beta(1 - \beta)Q^2} + \frac{k^2}{Q^2} \right]^{-1}.
\end{aligned} \tag{11}$$

Eqs. (8)–(10) enable us to evaluate the singlet quark distribution Σ in terms of the gluon f . We obtain

$$\begin{aligned}
\Sigma(x, k^2) &= S_{\text{non-p}}(x) + \sum_q \int_x^a \frac{dz}{z} S_q^{\text{box}}(z, \kappa'^2 = 0, k^2) \frac{x}{z} g\left(\frac{x}{z}, k_0^2\right) \\
&+ \sum_q \int_{k_0^2}^{\infty} \frac{dk'^2}{k'^2} \int_x^1 \frac{dz}{z} S_q^{\text{box}}(z, \kappa'^2, k^2) f\left(\frac{x}{z}, k'^2\right) + V(x, k^2) \\
&+ \int_{k_0^2}^{k^2} \frac{dk'^2}{k'^2} \frac{\alpha_S(k'^2)}{2\pi} \int_x^1 dz P_{qq}(z) S_{uds}\left(\frac{x}{z}, k'^2\right)
\end{aligned} \tag{12}$$

where $a = (1 + 4m_q^2/Q^2)^{-1}$ and $V = x(u_v + d_v)$. Here we have separated off the non-perturbative contributions. $S_{\text{non-p}}$ is the contribution from the region $k^2, \kappa'^2 < k_0^2$ and the next term is the contribution from the region $k^2 < k_0^2 < \kappa'^2$. The details are explained in ref. [7]. An $S \rightarrow S$ contribution (from the light u, d, s quarks) is also included. For the light u, d, s quarks $S_q^{\text{box}}(z, \kappa'^2 = 0, k^2)$ in (12) is defined with the κ'^2 integration restricted to the region $\kappa'^2 > k_0^2$.

In this way coupled integral equations are obtained for the unintegrated gluon $f(x, k^2)$ and the integrated quark singlet $\Sigma(x, k^2)$ distributions. The driving terms are specified by an economically parametrized non-perturbative contribution $S_{\text{non-p}}(x)$ and by the integrated gluon distribution at scale $k_0^2 = 1 \text{ GeV}^2$ which was taken to be of the form

$$xg(x, k_0^2) = N(1 - x)^\beta. \tag{13}$$

The valence distribution $V(x, k^2)$ was taken from the parton set of ref. [16]. With this input the coupled equations (6) and (12) were solved and a fit made of the deep inelastic electron-proton F_2 data obtained by the H1, ZEUS, NMC and BCDMS collaborations [7]. An excellent description of these data was obtained with physically reasonable values of the parameters: $N = 1.57$ and $\beta = 2.5$. Incidentally, the output gluon at $x \sim 0.4$ was reasonably compatible with the expectations of prompt photon data. In summary, ref. [7] gives an unintegrated gluon distribution and, through k_T factorization, a sea distribution which can be reliably extrapolated to very low values of x .

3. The neutrino cross sections

Here we collect together all the relevant formulas which are needed to calculate the cross sections for neutrino-nucleon interactions. We express the cross sections in terms of the structure functions for an isoscalar nucleon target, $N = (n + p)/2$, [17, 18, 19]

$$\begin{aligned} \frac{d^2\sigma^{\nu,\bar{\nu}}}{dxdy} &= \frac{G_F ME}{\pi} \left(\frac{M_i^2}{Q^2 + M_i^2} \right)^2 \left\{ \frac{1 + (1 - y)^2}{2} F_2^\nu(x, Q^2) \right. \\ &\quad \left. - \frac{y^2}{2} F_L^\nu(x, Q^2) \pm y \left(1 - \frac{y}{2} \right) x F_3^\nu(x, Q^2) \right\} \end{aligned} \quad (14)$$

where G_F is the Fermi coupling constant, M is the proton mass, E is the laboratory energy of the neutrino and $y = Q^2/xs$. The mass M_i is either M_W or M_Z according to whether we are calculating charged current (CC) or neutral current (NC) neutrino interactions.

We may express the structure functions F_i in terms of the valence and sea quark momentum distributions, V_q and S_q , of (10). For the charged current νN interaction we have

$$F_2^{\text{CC}} = x(u_v + d_v) + S_u + S_d + 2x(s + c + b + t), \quad (15)$$

where the heavy quark contributions are calculated from the photon-gluon fusion mechanism. To be precise for the $s \rightarrow c$ and $\bar{c} \rightarrow \bar{s}$ contributions we use

$$\begin{aligned} 2xq(x, Q^2) &= \int_x^{a_c(k^2=0)} \frac{dz}{z} S_q^{\text{box}}(z, k^2 = 0, Q^2) \frac{x}{z} g\left(\frac{x}{z}, k_0^2\right) \\ &\quad + \int_{k_0^2}^{\infty} \frac{dk^2}{k^2} \int_x^{a_c(k^2)} \frac{dz}{z} S_q^{\text{box}}(z, k^2, Q^2) f\left(\frac{x}{z}, k^2\right) \end{aligned} \quad (16)$$

with $q = s$ or c and with S_q^{box} defined by (10) with $m_q = 0$. However the mass is included in the threshold factor

$$a_c(k^2) = \left[1 + \frac{k^2 + m_c^2}{Q^2} \right]^{-1}. \quad (17)$$

For the small $b \rightarrow t$ and $\bar{t} \rightarrow \bar{b}$ contributions we use the standard on-shell factorization formula

$$2xq(x, Q^2) = \int_x^a \frac{dz}{z} H(z, m_q, m_{q'}, Q^2) \frac{x}{z} g\left(\frac{x}{z}, \hat{s}\right) \quad (18)$$

with $q = b$ or t (and $q' = t$ or b) and where the scale $\hat{s} = Q^2(1 - z)/z$ and

$$a = [1 + (m_t + m_b)^2/Q^2]^{-1}. \quad (19)$$

The functions H are defined in ref. [20]

$$\begin{aligned} F_3^{\text{CC}} &= u_v + d_v \\ F_L^{\text{CC}} &= B_u + B_d + \frac{4\alpha_S(Q^2)}{3\pi} \int_x^1 dy \left(\frac{x}{y} \right)^2 F_2^{\text{CC}}(y, Q^2). \end{aligned} \quad (20)$$

The function B_q describes the boson-gluon fusion contribution to F_L

$$\begin{aligned} B_q(x, Q^2) &= \frac{\alpha_S(Q^2)}{\pi} \int_x^1 \frac{dy}{y} \frac{x}{y} \left(1 - \frac{x}{y}\right) yg(y, k_0^2) \\ &\quad + \frac{Q^4}{\pi^2} \int_{k_0^2} \frac{dk^2}{k^4} \int_0^1 d\beta \beta^2 (1 - \beta)^2 \int d^2 \kappa' \left(\frac{1}{D_{1q}} - \frac{1}{D_{2q}}\right)^2 f\left(\frac{x}{z_0}, k^2\right) \end{aligned} \quad (21)$$

where D_{iq} and z_0 are given in (11). Besides B_u and B_d , there is also boson-gluon production of heavy quarks which may be treated similarly to that for F_2^{CC} .

The structure functions for the neutral current νN interaction are

$$F_2^{\text{NC}} = (L_u^2 + L_d^2 + R_u^2 + R_d^2) \frac{1}{4} \left\{ \sum_q S_q + xu_v + xd_v \right\}, \quad (22)$$

where the sum over S_q is given by the first three terms on the right hand side of (12), and

$$\begin{aligned} F_3^{\text{NC}} &= (L_u^2 + L_d^2 - R_u^2 - R_d^2) \frac{1}{4} (u_v + d_v) \\ F_L^{\text{NC}} &= (L_u^2 + L_d^2 + R_u^2 + R_d^2) \frac{1}{4} \sum_q B_q + \frac{4\alpha_S(Q^2)}{3\pi} \int_x^1 dy \left(\frac{x}{y}\right)^2 F_2^{\text{NC}}(y, Q^2) \end{aligned} \quad (23)$$

where the chiral couplings are

$$\begin{aligned} L_u &= 1 - \frac{4}{3} \sin^2 \theta_W, & L_d &= -1 + \frac{2}{3} \sin^2 \theta_W, \\ R_u &= -\frac{4}{3} \sin^2 \theta_W, & R_d &= \frac{2}{3} \sin^2 \theta_W. \end{aligned} \quad (24)$$

The parton distributions that are used to evaluate the neutrino cross sections are those described in Section 2, which are obtained by solving the unified BFKL/DGLAP equations with higher order $\ln 1/x$ effects incorporated via the consistency condition. The various components of the CC and NC neutrino cross sections are shown as a function of the laboratory neutrino energy in Figs. 2 and 3 respectively. In each case we see that for neutrino energies $E > 10^5$ GeV the sea quark contributions dominate over the valence. The rise of the sea distributions with decreasing x is reflected in the continued rise of the sea components of the cross section with energy. We also note that for $E > 10^5$ GeV the valence component of the cross section becomes independent of energy. This results from the fact that when (14) is integrated over x and y , or to be precise over x and Q^2 , the Q^2 integration is effectively cut-off at $Q^2 \sim M_i^2$, together with the fact that the number of valence quarks is finite. The threshold effects of the heavy quark contributions are also evident in Figs. 2 and 3. We combine the charged current and neutral current cross sections in Fig. 4.

In ref. [7] we also solved the unified equation with the omission of non-leading effects arising from the consistency condition. Using those partons we obtain higher cross sections at ultrahigh

energies as illustrated by the dashed curve in Fig. 5. Of course this is only shown for comparison since it is based on LO BFKL which is an unreliable approximation [8]. Therefore throughout this paper we impose the consistency constraint (4) which generates the dominant non-leading $\ln(1/x)$ effects. In Fig. 6 a comparison is made with other recent calculations of the νN total cross section [4, 5] based on NLO DGLAP evolution, with BFKL and higher order $\ln(1/x)$ effects neglected. We see that our results and those of [4, 5] are remarkably similar considering their different dynamic origin. Since we include resummation of $\ln(1/x)$ effects we expect the continuous curve to give the most reliable extrapolation to ultrahigh energies. In fact we may conclude from a comparison of (3) and (5) that our all-order sub-leading $\ln(1/x)$ treatment gives an upper estimate of the cross sections. Considering that the predictions are so similar, although they are based on different dynamical assumptions, we may conclude that the ambiguity in extrapolating the neutrino cross sections to ultrahigh energies is less than might at first be expected.

At ultrahigh energies the antineutrino cross sections are essentially identical to the neutrino cross sections, since the difference is due to the structure function F_3 which is controlled by valence quarks. In Table I we list the various cross sections as a function of energy.

To gain insight into the (x, Q^2) domain that is sampled by ultrahigh energy neutrinos we show plots in Fig. 7 in which the contours enclose regions contributing different fractions of the total cross section. The two plots illustrate the dependence of the domains on the neutrino energy. For the ultrahigh energy chosen for Fig. 7(b) we see that the main contribution comes from the domain $Q^2 \simeq M_W^2$ and $x \sim M_W^2/(2ME)$, where M is the proton mass, as anticipated from (14). For the lower energy used in Fig. 7(a) some residual propagator effects are still apparent and $Q^2 \lesssim M_W^2$ and $x \lesssim M_W^2/2ME$.

4. Transport equations

The ultrahigh energy neutrinos when penetrating through the Earth can undergo attenuation due to charged and neutral current interactions as well as the regeneration due to the neutral current interactions at higher energies. Both effects are summarized in the transport equation for the neutrino flux $I(E, \tau)$ [9, 10]:

$$\frac{dI(E, \tau)}{d\tau} = -\sigma_{\text{TOT}}(E)I(E, \tau) + \int \frac{dy}{1-y} \frac{d\sigma_{\text{NC}}(E', y)}{dy} I(E', \tau) \quad (25)$$

where $\sigma_{\text{TOT}} = \sigma_{\text{CC}} + \sigma_{\text{NC}}$ and where y is, as usual, the fractional energy loss such that

$$E' = \frac{E}{1-y}. \quad (26)$$

The variable τ is the number density of nucleons n integrated along a path of length z through the Earth

$$\tau = \int_0^z dz' n(z'). \quad (27)$$

The number density $n(z)$ is defined as $n(z) = N_A \rho(z)$ where $\rho(z)$ is the density of Earth along the neutrino path length z and N_A is the Avogadro number. Clearly the number of nucleons τ encountered along the path z depends upon the nadir angle θ between the normal to the Earth's surface (passing through the detector) and the direction of the neutrino beam incident on the detector. For example $\theta = 0^\circ$ corresponds to a beam transversing the diameter of the Earth. To compute the variation of τ with the angle θ we need to know the density profile of the Earth. We use the preliminary Earth model [21].

It is convenient to represent the solution of the transport equation (25) in the form:

$$I(E, \tau) = I_0(E) \exp(-\sigma_{\text{TOT}}(E)\tau) \Psi(E, \tau) \quad (28)$$

where $I_0(E)$ denotes the flux of neutrinos incident on the surface of the Earth from outer space. The function $\Psi(E, \tau)$ would be unity in the absence of regeneration. It satisfies the following equation:

$$\frac{d\Psi(E, \tau)}{d\tau} = \int \frac{dy}{1-y} \frac{I_0(E')}{I_0(E)} \exp[-(\sigma_{\text{TOT}}(E') - \sigma_{\text{TOT}}(E))\tau] \frac{d\sigma_{\text{NC}}(E', y)}{dy} \Psi(E', \tau), \quad (29)$$

with the initial condition $\Psi(z, \tau = 0) = 1$. We solve this equation numerically and determine the regeneration factor Ψ as a function of E and τ . The solution is sensitive to the behaviour of σ_{TOT} for $E' > E$ and on energy dependence of the initial flux $I_0(E)$ and on the value of $d\sigma_{\text{NC}}/dy$. In particular the flatter the initial spectrum $I_0(E)$ the more it is possible to sample $d\sigma/dy$ at energies E' much higher than E and so the amount of regeneration is increased. In practice the result is a combined effect of the fall-off due to I_0 and the experimental attenuation and the enhancement due to $d\sigma_{\text{NC}}/dy$. To illustrate the general properties of the solution we show the shadowing factor,

$$S = \Psi(E, \tau) \exp(-\sigma_{\text{TOT}}(E)\tau), \quad (30)$$

of (28) for two different, but physically relevant, forms of the initial flux. First we consider the flux of atmospheric neutrinos given by [22]

$$I_0(E) = cE^{-3.6}, \quad (31)$$

which has a rapid fall-off with energy, and second, we consider the flux from Active Galactic Nuclei (AGN) as given by ref. [23] for which the incident flux $I_0(E)$ is approximately constant throughout the interval $10^3 < E < 10^5$ GeV. The results are presented by the continuous curves in Fig. 8 for three different incident directions, $\theta = 0^\circ, 40^\circ$ and 80° , corresponding to values of $\tau/N_A = 1.1 \times 10^{10}, 0.45 \times 10^{10}$, and 0.072×10^{10} cmwe respectively. For illustration we also show, by dashed curves, the pure attenuation factors $A \equiv \exp(-\sigma_{\text{TOT}}\tau)$ with regeneration omitted. Since the neutrino cross sections increase with energy we observe that the attenuation factor A leads to total shadowing once the energy is sufficiently high. The energy at which this occurs depends mainly on τ . The regeneration, which increases the flux at the detector, is

sensitive to the energy dependence of I_0 . For a steeply falling flux, corresponding, for example, to atmospheric neutrinos, regeneration gives a rather small effect. On the other hand for a flatter initial flux $I_0(E)$ the regeneration effect can be quite significant. In fact it can even enhance the initial flux by as much as 40%, as can be seen from the shadowing factor at $\theta = 0^\circ$ for the AGN flux used in Fig. 6. A similar result was found in ref. [9]. In the next section we present the flux arriving at the detector from various sources for a range of angles taking into account the full shadowing factor of (28).

5. Penetration of the Earth for given incident fluxes

The initial incident neutrino flux $I_0(E)$ is modified on its passage through the Earth by the shadowing factor S of (30). For experimental purposes the relevant quantity is the neutrino flux $I(E)$ reaching the detector at different nadir angles θ . The four plots in each of Figs. 9 and 10 show first the initial flux $I_0(E)$ and then the flux at the detector $I(E)$ for the three nadir angles $\theta = 80^\circ, 40^\circ$ and 0° . Recall that 0° is penetration of neutrinos through the centre of the Earth. The various curves are for neutrinos of different origin. For convenience of reference we show the atmospheric neutrino flux in both Figs. 9 and 10. In Fig. 9 we compare this background spectrum with three different models of the flux expected from Active Galactic Nuclei (AGN) [23, 24, 25]. The AGN flux stands out above the atmospheric neutrino background for neutrino energies above about 10^5 GeV. However the AGN spectrum is attenuated at ultrahigh neutrino energies by shadowing. The smaller the nadir angle θ the greater the shadowing. For example at $\theta = 80$ or 40° the weighted flux EdN/dE falls below $10^{-15} \text{ cm}^{-2} \text{ s}^{-1} \text{ sr}^{-1}$ at $E \sim 10^8$ and 10^7 GeV respectively. Fig. 10 shows the corresponding fluxes for neutrinos coming from gamma ray bursts [26] and from a sample top-down model [27]. Similar attenuation can be observed in Fig. 10 to that in Fig. 9.

So far we have discussed the effects generated by inelastic neutrino interactions with hadronic matter. Another possible source of modification of the neutrino fluxes which penetrate the Earth may be due to neutrino oscillations [28, 29, 30, 31]. The properties of neutrino oscillations in matter have been discussed in [32]. They are characterised by an effective oscillation length ℓ_m and mixing angle θ_m which differ from those in vacuum, which we denote ℓ_v and θ_v . To be precise in the MSW model for mixing of two neutrino species we have

$$\ell_m = \ell_v \left[1 + 2 \frac{\ell_v}{\ell} \cos \theta_v + \frac{\ell_v^2}{\ell^2} \right]^{-\frac{1}{2}} \quad (32)$$

$$\tan 2\theta_m = \frac{\sin 2\theta_v}{\cos 2\theta_v + (\ell_v/\ell)} \quad (33)$$

where ℓ originates from the matter contribution to the oscillation length and is given by

$$\ell = \frac{\sqrt{2}\pi}{G_F n_e} = \frac{1.77 \times 10^7}{\rho_e} \text{ m} \quad (34)$$

where n_e is the electron density and ρ_e is the number density in units of Avogadro's number/cm³. An important property of ℓ_m is that it saturates at the value ℓ given by (34) [33]. That is

$$(\ell_m)_{\max} = \ell \simeq 10^3 - 10^4 \text{ km} \quad (35)$$

for matter oscillations in the Earth with $\rho_e = 2 - 10$. This is in contrast with the oscillation length in vacuum

$$\ell_v = 4\pi E/\Delta m_\nu^2 \quad (36)$$

which increases with increasing energy. Most importantly we see that at sufficiently high energy ℓ_v/ℓ becomes very large and the effective mixing angle θ_m tends to zero, see (33). In fact for the very small values of the mass difference of the neutrinos ($\Delta m_\nu^2 \simeq 10^{-6} \text{ eV}^2$ suggested by the data [30]) we can safely neglect the modification of the neutrino fluxes due to neutrino oscillations in their passage through the Earth for $E > 1 \text{ TeV}$ or so. Of course neutrino oscillations can, in principle, modify the flux $I_0(E)$ arriving at the Earth.

6. Conclusions

In this paper we have extended the recently developed [7] unified BFKL/DGLAP framework to calculate the total cross sections of ultrahigh neutrino interactions with nucleons. The framework incorporated non-leading $\ln(1/x)$ effects which are generated by the consistency condition given in (4). In this way it was possible to resum to all orders the dominant part of the non-leading $\ln(1/x)$ effects and to obtain a physically acceptable description of the structure functions at low x . Indeed this unified BFKL/DGLAP approach gave an excellent description of the F_2 data from HERA and enables us to extrapolate the structure functions to the region of the very small values of x which are probed in the ultrahigh energy neutrino interactions. We compared our predictions for the cross sections with the results of the two recent calculations which were obtained within the NLO DGLAP framework. We find that all three approaches give results for the neutrino cross sections within 30% - 40% or so. We may conclude that the potential ambiguities in the extrapolation of the cross sections are much smaller than might have been expected. However the present calculation, which includes a treatment of $\ln(1/x)$ effects at small x , should be the more reliable for ultrahigh energy neutrino interactions. It should be stressed that the inclusion of the dominant non-leading $\ln(1/x)$ effects was crucial for obtaining this result. Extrapolation based on the LO BFKL equation would generate cross sections which would be enhanced by a factor of more than two at ultrahigh neutrino energies $E_\nu \sim 10^{12} \text{ GeV}$. This LO approximation is, however, known to be unreliable.

The calculated neutrino cross sections were next used as an input in the transport equation describing the modification of the neutrino flux during the penetration of the Earth. This equation incorporated both the attenuation effects of the neutrino "beam" as well as the regeneration of neutrinos due to neutral current interactions. We solved the equation for a variety of initial neutrino fluxes and discussed the dependence of the shadowing factor upon the nadir angle θ . We found that although attenuation of the neutrino flux is the major effect, nevertheless enhancement due to neutrino regeneration can become appreciable for fluxes which extend

to the very high neutrino energies, like those originating from AGN sources. The calculations of the neutrino fluxes at various nadir angles show that at sufficiently high energies neutrinos become strongly attenuated. The smaller the nadir angle the lower the energy of complete attenuation.

To sum up we have demonstrated that a framework which incorporates QCD expectations at low x , including the BFKL effects with the resummation of the non-leading $\ln(1/x)$ terms, gives neutrino cross sections which are compatible with those obtained within the NLO DGLAP framework. This strongly limits potential ambiguities in the possible values of the cross sections extrapolated from the HERA domain to the region of x and Q^2 which can be probed in ultrahigh energy neutrino interactions. Due to large values of these cross sections the attenuation effects reduce the fluxes of ultrahigh energy neutrinos particularly at small nadir angles. Nevertheless there is a window for the observation of AGN by km³ underground detectors of the energetic decay muons. We have found that the AGN flux exceeds the atmospheric neutrino background for neutrinos energies $E \gtrsim 10^5$ GeV. Typical results are shown in Fig. 9. These illustrate the possibility of observing AGN at various nadir angles by “neutrino astronomy”.

Acknowledgements

We thank Francis Halzen and Argyris Nicolaïdis for stimulating our interest in this problem. We thank them and Ron Girdler, Karl Mannheim, Floyd Stecker and Ubi Wiczoski for useful discussions and correspondence. Günter Sigl is thanked for providing data files for neutrino fluxes. JK and AMS thank the Physics Department and Grey College of the University of Durham for their warm hospitality. JK thanks the UK PPARC for a Visiting Fellowship. This research has been supported in part by the Polish State Committee for Scientific Research (KBN) grants N0 2 P03B 89 13, 2 P03B 137 14 and by the EU Fourth Framework Programme “Training and Mobility of Researchers”, Network “Quantum Chromodynamics and the Deep Structure of Elementary Particles”, contract FMRX - CT98 - 0194.

References

- [1] See, for example, T. K. Gaisser, F. Halzen and T. Stanev, Phys. Reports **258** (1995) 173; F. Halzen, Lectures on Neutrino Astronomy, TASI School, 1998, MADPH-98-1088.
- [2] A. M. Cooper-Sarkar, R. C. E. Devenish and A. De Roeck, Int. J. Mod. Phys. **A13** (1998) 3385, and references therein.
- [3] R. Gandhi, C. Quigg, M. Reno and I. Sarcevic, Astropart. Phys. **5** (1996) 81.
- [4] R. Gandhi, C. Quigg, M. Reno and I. Sarcevic, Phys. Rev. **D58** (1998) 093009.
- [5] M. Glück, S. Kretzer and E. Reya, DO-TH-98-20, [astro-ph/9809273](#).
- [6] E.A. Kuraev, L.N. Lipatov and V.S. Fadin, Sh. Eksp. Teor. Fiz. **72** (1977) 373, (Sov. Phys. JETP **45** (1977) 199); Ya. Ya. Balitzkij and L.N. Lipatov, Yad. Fiz. **28** (1978) 1597 (Sov. J. Nucl. Phys. **28** (1978) 822), J.B. Bronzan and R.L. Sugar, Phys. Rev. **D17** (1978) 585; T. Jaroszewicz, Acta. Phys. Polon. **B11** (1980) 965.
- [7] J. Kwiecinski, A.D. Martin and A.M. Stasto, Phys. Rev. **D56** (1997) 3991; J. Kwiecinski, A.D. Martin and A.M. Stasto, Acta Phys. Polon. **B28**, No.12 (1997) 2577.
- [8] L. N. Lipatov and V. S. Fadin, Sov. J. Nucl. Phys. **50** (1989) 712; V.S. Fadin, R. Fiore and M.I. Kotsky, Phys. Lett. **B339** (1995) 181; Phys. Lett. **B387** (1996) 593; Phys. Lett. **B389** (1996) 737; V. S. Fadin and L. N. Lipatov, Nucl. Phys. **B406** (1993) 259; Nucl. Phys. **B477** (1996) 767; [hep-ph/9802290](#); V. S. Fadin, R. Fiore and A. Quartarolo, Phys. Rev. **D50** (1994) 5893; V. S. Fadin, M. I. Kotsky and L. N. Lipatov, Phys. Lett. **B415** (1997) 97; V. Del Duca, Phys. Rev. **D54** (1996) 989; Phys. Rev. **D54** (1996) 4474; V. Del Duca and C. R. Schmidt, Phys. Rev. **D57** (1998) 4069; [hep-ph/9810215](#); V. S. Fadin, R. Fiore, A. Flashi and M. I. Kotsky, Phys. Lett. **B422** (1998) 287; M. Ciafaloni, Phys. Lett. **B429** (1998) 363; G. Camici and M. Ciafaloni, Phys. Lett. **B386** (1996) 341; Phys. Lett. **B395** (1997) 118; Phys. Lett. **B412** (1997) 396, Erratum-ibid. **B417** 390; Phys. Lett. **B430** (1998) 349; Nucl. Phys. **B496** (1997) 305; [hep-ph/9803389](#); M. Ciafaloni and D. Colferai, [hep-ph/9806350](#); D. A. Ross, Phys. Lett. **B431** (1998) 161.
- [9] A. Nicolaïdis and A. Taramopoulos, Phys. Lett. **B386** (1996) 211.
- [10] V. A. Naumov and L. Perrone, [hep-ph/9804301](#).
- [11] G. C. Hill, Astropart. Phys. **6** (1997) 215.

- [12] J. Kwiecinski, A.D. Martin and P.J. Sutton, *Z. Phys. C* **71** (1996) 585.
- [13] B. Andersson, G. Gustafson and J. Samuelsson, Lund preprint, LU-TP 95-13;
B. Andersson, G. Gustafson, H. Kharraziha and J. Samuelsson, *Z. Phys. C* **71** (1996) 613.
- [14] G.P. Salam, *J. High Energy Phys.* **9807** (1998) 019.
- [15] S. Catani, M. Ciafaloni and F. Hautmann, *Phys. Lett. B* **242** (1990) 97; *Nucl. Phys.* **366** (1991) 657;
J.C. Collins and R.K. Ellis, *Nucl. Phys. B* **360** (1991) 3;
S. Catani and F. Hautmann, *Nucl. Phys. B* **427** (1994) 475;
M. Ciafaloni, *Phys. Lett. B* **356** (1995) 74.
- [16] M. Glück, E. Reya and A. Vogt, *Z. Phys. C* **67** (1995) 433.
- [17] R. G. Roberts, The structure of the proton: Deep inelastic scattering, Cambridge University Press, Cambridge, 1990.
- [18] F. Halzen and A. D. Martin, Quarks and Leptons: An introductory course in modern Particle Physics, John Wiley and Sons, 1984.
- [19] R. K. Ellis, W. J. Stirling and B. R. Webber, QCD and collider physics, Cambridge University Press, Cambridge, 1996.
- [20] M. Glück, R.M. Godbole and E. Reya, *Z. Phys. C* **38** (1988) 441, Erratum-*ibid. C* **39** (1988) 590.
- [21] A.M. Dziewonski and D.L. Anderson, Preliminary Reference Earth Model, *Physics Earth and Planetary Interiors*, **25** (1981) 297.
- [22] L.V. Volkova, *Yad. Fiz.* **31** (1980) 1510, (Sov. J. Nucl. Phys. **31** (1980) 784.)
- [23] R. J. Protheroe, Accretion Phenomena and Related Outflows, IAU Colloq.163, ed. D. Wickramasinghe et al., 1996, [astro-ph/9607165](#); Talk at Neutrino 98, Takayama 4-9 June 1998, [astro-ph/9809144](#); ADP-AT-96-15, Towards the Millennium in Astrophysics: Problems and Prospects, Erice 1996, eds. M.M. Shapiro and J.P. Wefel (World Scientific, Singapore), [astro-ph/9612213](#).
- [24] K. Mannheim, *Astroparticle Physics* **3** (1995) 295.
- [25] F.W. Stecker and M.H. Salamon, “TeV Gamma-ray Astrophysics” (1994) 341, [astro-ph/9501064](#)
- [26] E. Waxman and J. Bahcall, *Phys. Rev. Lett.* **78**, (1997) 2292.

- [27] G. Sigl, S. Lee, P. Bhattacharjee and S. Yoshida, [hep-ph/9809242](#) to appear in Phys. Rev D.;
 G. Sigl, S. Lee, D. N. Schramm and P. Coppi, Phys. Lett. **B392** (1997) 129, [astro-ph/9610221](#).
- [28] GALLEX Collaboration (P. Anselmann et al.), Phys. Lett. **B357** (1995) 237; Erratum-ibid. **B361** (1996) 235; Phys. Lett. **B327** (1994) 377.
- [29] SAGE Collaboration, Nucl. Phys. Proc. Suppl. **48** (1996) 299; Phys. Lett. **B328** (1994) 234.
- [30] Kamiokande Collaboration, Y. Fukuda, Phys. Rev. Lett. **77** (1996) 1683.
- [31] The SuperKamiokande Collaboration, Y. Fukuda et al., Phys. Rev. Lett. **81** (1998) 1158; Erratum-ibid. **81** (1998) 4279; Phys. Rev. Lett. **81** (1998) 3319.
- [32] L. Wolfenstein, Phys. Rev. **D17**, (1978) 2369; S.P. Mikheyev and A.Yu. Smirnov, Yad. Fiz. **42**, (1985) 1441 [Sov. J. Nucl. Phys. **42** (1985) 913.]; Nuovo Cimento **C9**, 17 (1986), see also P. D. B. Collins, A. D. Martin and E. J. Squires in Particle Physics and Cosmology, Wiley, New York, 1989.
- [33] P. Lipari and M. Lusignoli, Phys. Rev. **D58** (1998) 073005.
- [34] H.L. Lai et al. (CTEQ collaboration), Phys. Rev. **D55**, (1997) 1280.

Table 1: The charged-current and neutral-current cross sections (in cm^2) for νN and $\bar{\nu} N$ interactions, where $N = \frac{1}{2}(p + n)$.

E_ν GeV	$\sigma_{\text{CC}}(\nu N)$	$\sigma_{\text{NC}}(\nu N)$	$\sigma_{\text{CC}}(\bar{\nu} N)$	$\sigma_{\text{NC}}(\bar{\nu} N)$
10^1	5.86×10^{-38}	1.81×10^{-38}	2.00×10^{-38}	7.54×10^{-39}
10^2	6.41×10^{-37}	1.99×10^{-37}	2.99×10^{-37}	1.05×10^{-37}
10^3	6.12×10^{-36}	1.94×10^{-36}	3.29×10^{-36}	1.16×10^{-36}
10^4	4.59×10^{-35}	1.55×10^{-35}	3.01×10^{-35}	1.07×10^{-35}
10^5	2.07×10^{-34}	7.33×10^{-35}	1.74×10^{-34}	6.20×10^{-35}
10^6	6.47×10^{-34}	2.28×10^{-34}	6.19×10^{-34}	2.18×10^{-34}
10^7	1.73×10^{-33}	5.95×10^{-34}	1.72×10^{-33}	5.90×10^{-34}
10^8	4.33×10^{-33}	1.45×10^{-33}	4.32×10^{-33}	1.45×10^{-33}
10^9	1.04×10^{-32}	3.38×10^{-33}	1.04×10^{-32}	3.38×10^{-33}
10^{10}	2.40×10^{-32}	7.61×10^{-33}	2.40×10^{-32}	7.61×10^{-33}
10^{11}	5.38×10^{-32}	1.66×10^{-32}	5.38×10^{-32}	1.66×10^{-32}
10^{12}	1.17×10^{-31}	3.53×10^{-32}	1.17×10^{-31}	3.53×10^{-32}

Figure Captions

Fig. 1 Diagrammatic representation of the k_T -factorization formula (2). At lowest order in α_S the gauge boson-gluon fusion processes, $Vg \rightarrow q\bar{q}$, are given by the quark box shown (together with the crossed box). The variables κ , k and k' denote the transverse momenta of the indicated virtual particles.

Fig. 2 The total νN charged current cross section and its decomposition into components of different origin as a function of the laboratory neutrino energy.

Fig. 3 The total νN neutral current cross section and its decomposition into components of different origin as a function of the laboratory neutrino energy.

Fig. 4 The total νN cross section together with its charged current and neutral current components as a function of the laboratory neutrino energy.

Fig. 5 The comparison of the total νN cross section calculated with and without the consistency constraint (4) imposed.

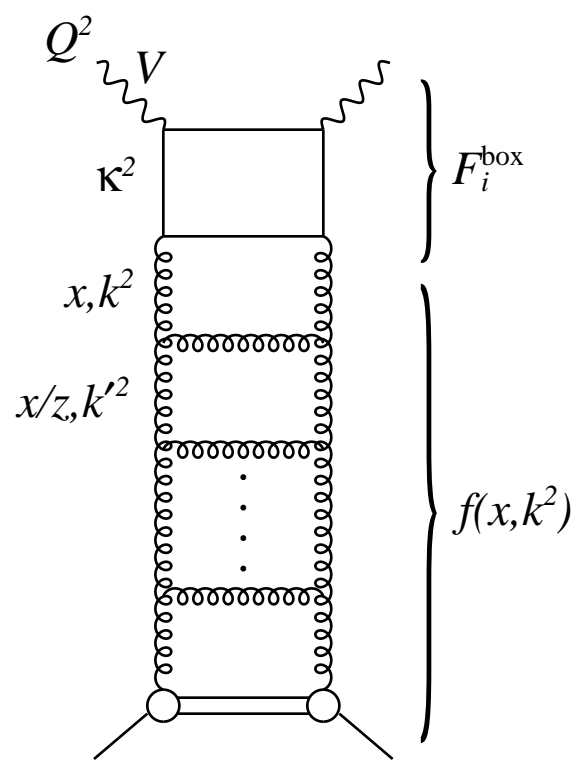
Fig. 6 The prediction for the total νN cross section obtained from a unified BFKL/DGLAP equation with (and, for comparison, without) the consistency condition imposed, compared to other recent calculations: [4] based on CTEQ parton distributions [34] and [5] based on GRV dynamical partons [16].

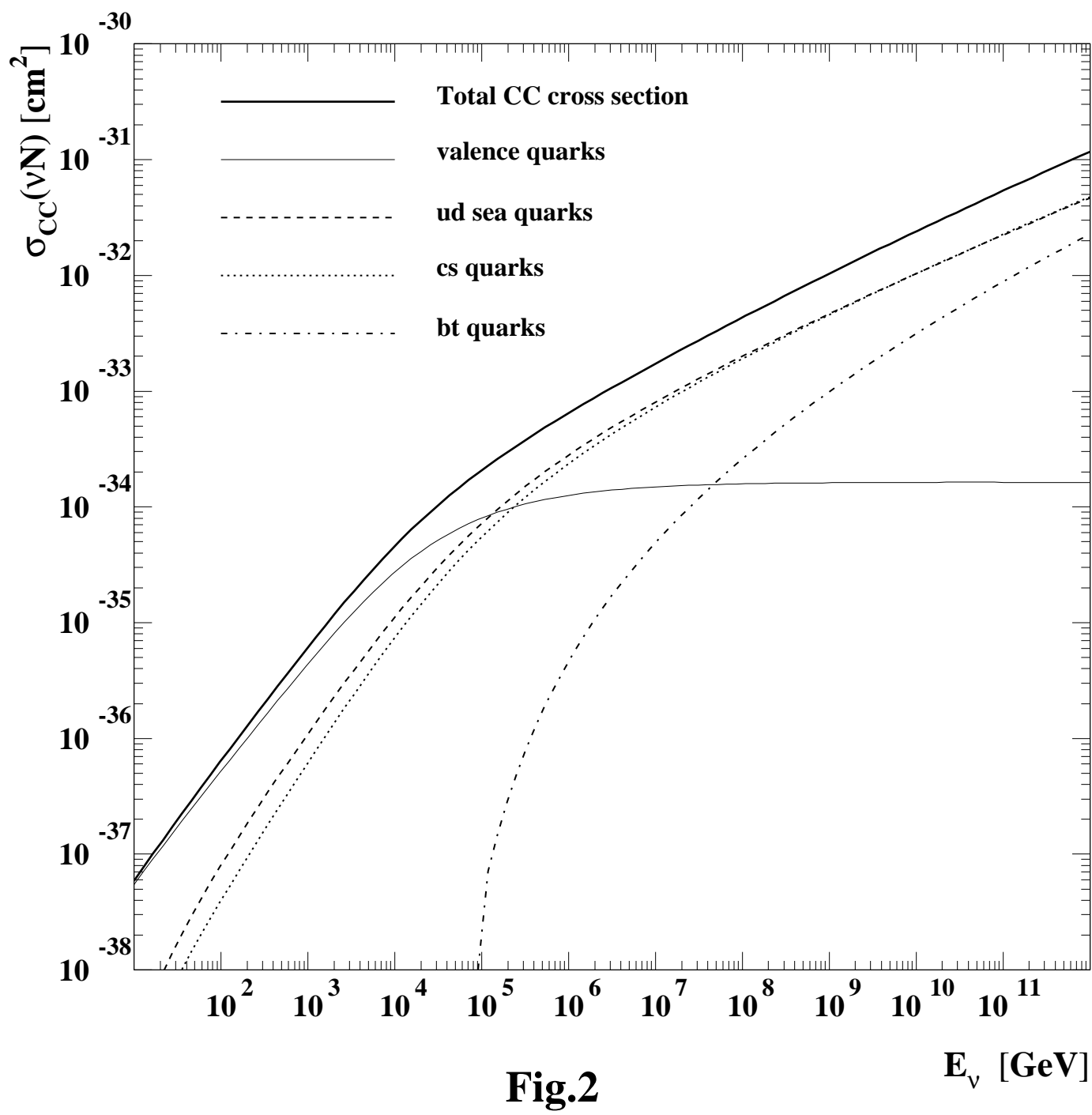
Fig. 7 A contour plot showing the x, Q^2 domain of the dominant contribution to the $d\sigma/d\ln(1/x)d\log Q^2$ for the total νN interaction at two values of the neutrino laboratory momentum: (a) $E_\nu = 10^6$ GeV and (b) $E_\nu = 10^{11}$ GeV. The 20 contours are such that they enclose a contribution of 5, 10, 15 … % of the above differential cross section.

Fig. 8 The shadowing factor S of (28) for two different initial neutrino fluxes incident at three different nadir angles on a detector. The angle $\theta = 0^\circ$ corresponds to penetration right through the Earth's diameter. The two curves on each plot show the shadowing factor with and without NC regeneration included.

Fig. 9 The initial flux $I_0(E)$ and the flux at the detector $I(E)$ for three different nadir angles corresponding to three models for AGN neutrinos [23, 24, 25]. The background atmospheric neutrino flux is also shown. All the fluxes are given for muon neutrinos. The corresponding fluxes from [23, 24, 25] were given originally for muon neutrinos and anti-neutrinos, and their value has been divided by factor 2.

Fig. 10 As for Fig. 9, but showing neutrino fluxes from gamma ray bursts [26] and from a top-down model [27]. All the fluxes are given for muon neutrinos. The corresponding fluxes from [26, 27] were given originally for muon neutrinos and anti-neutrinos, and their value has been divided by factor 2.





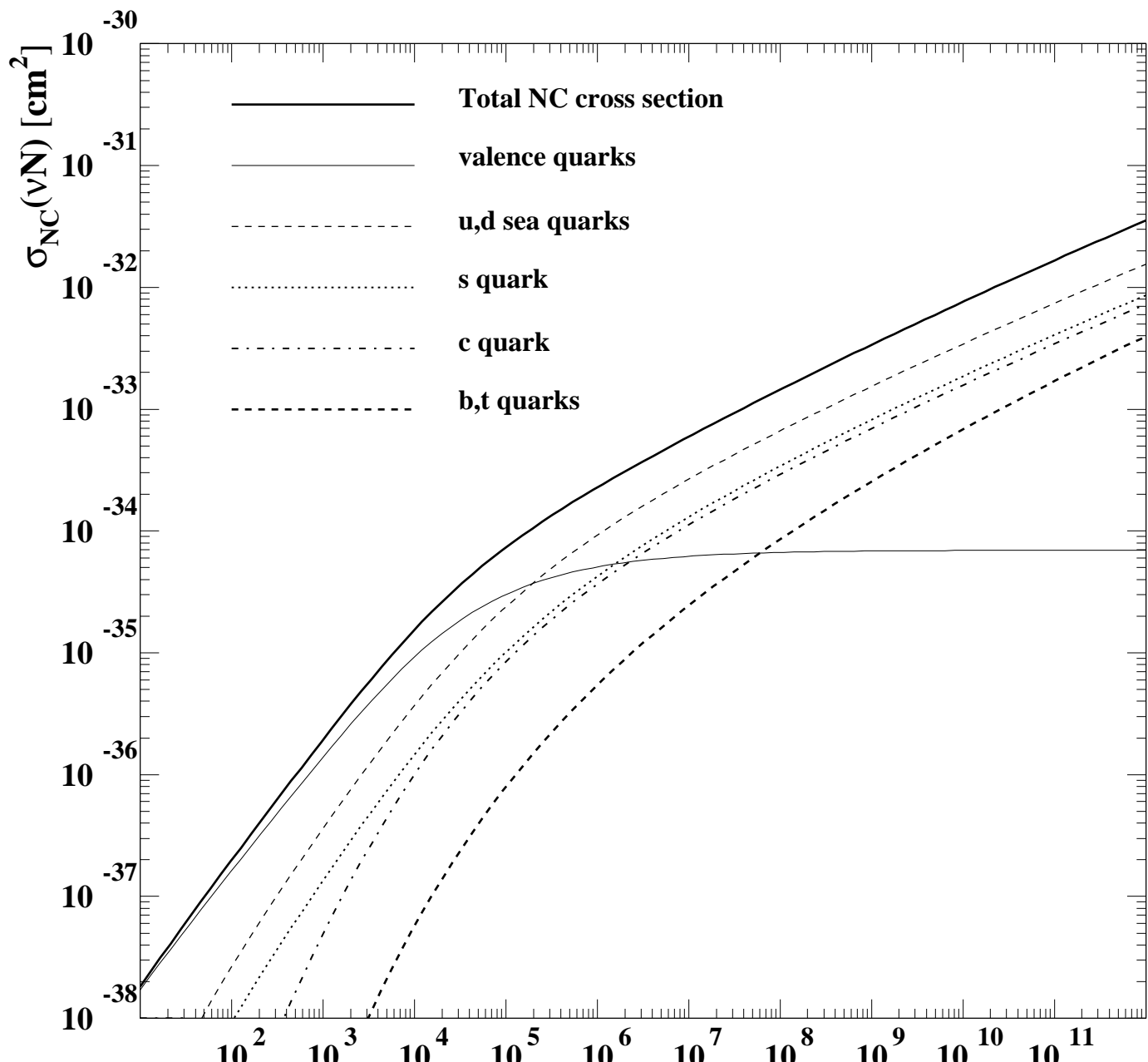


Fig.3

$E_v [\text{GeV}]$

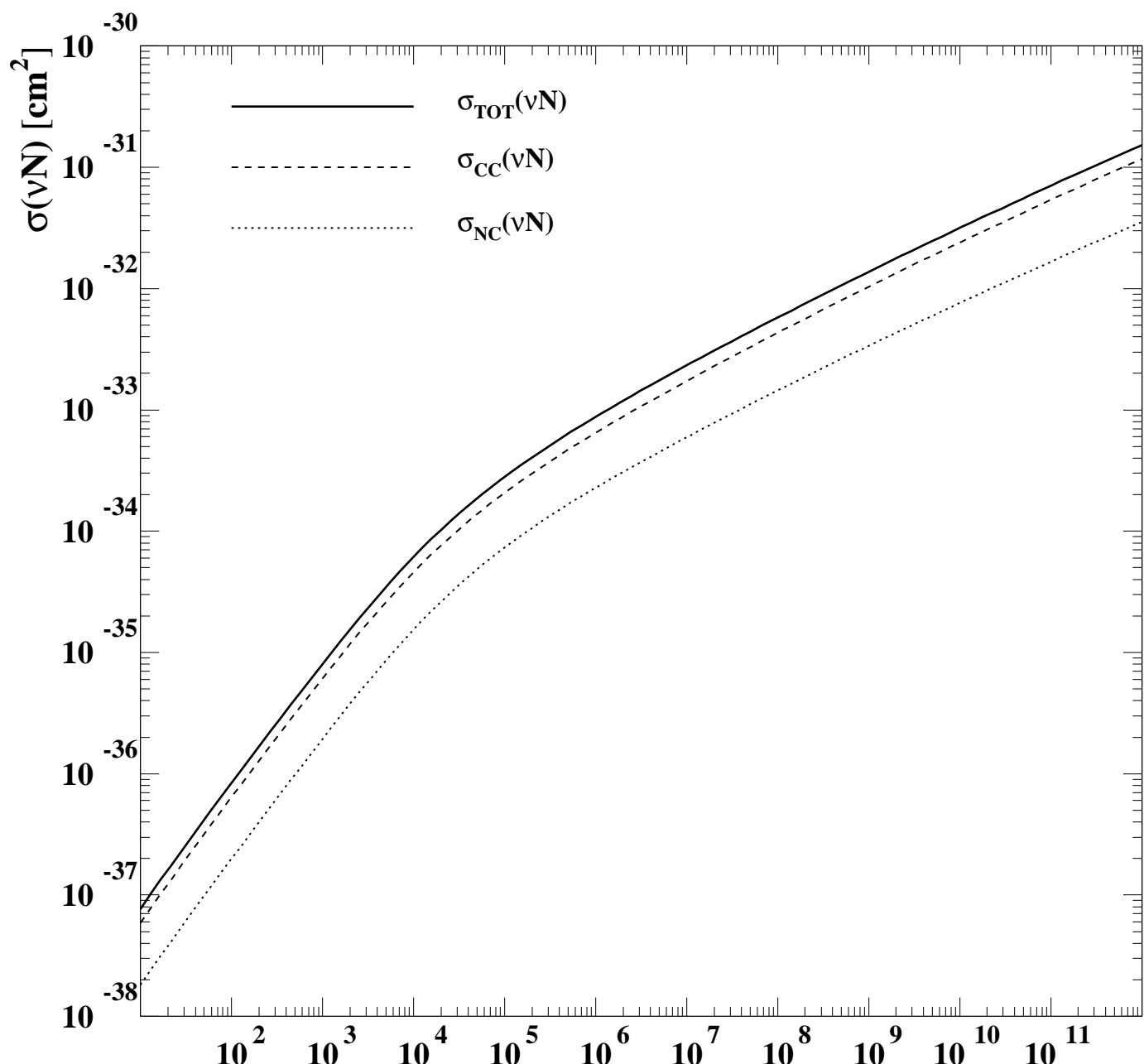
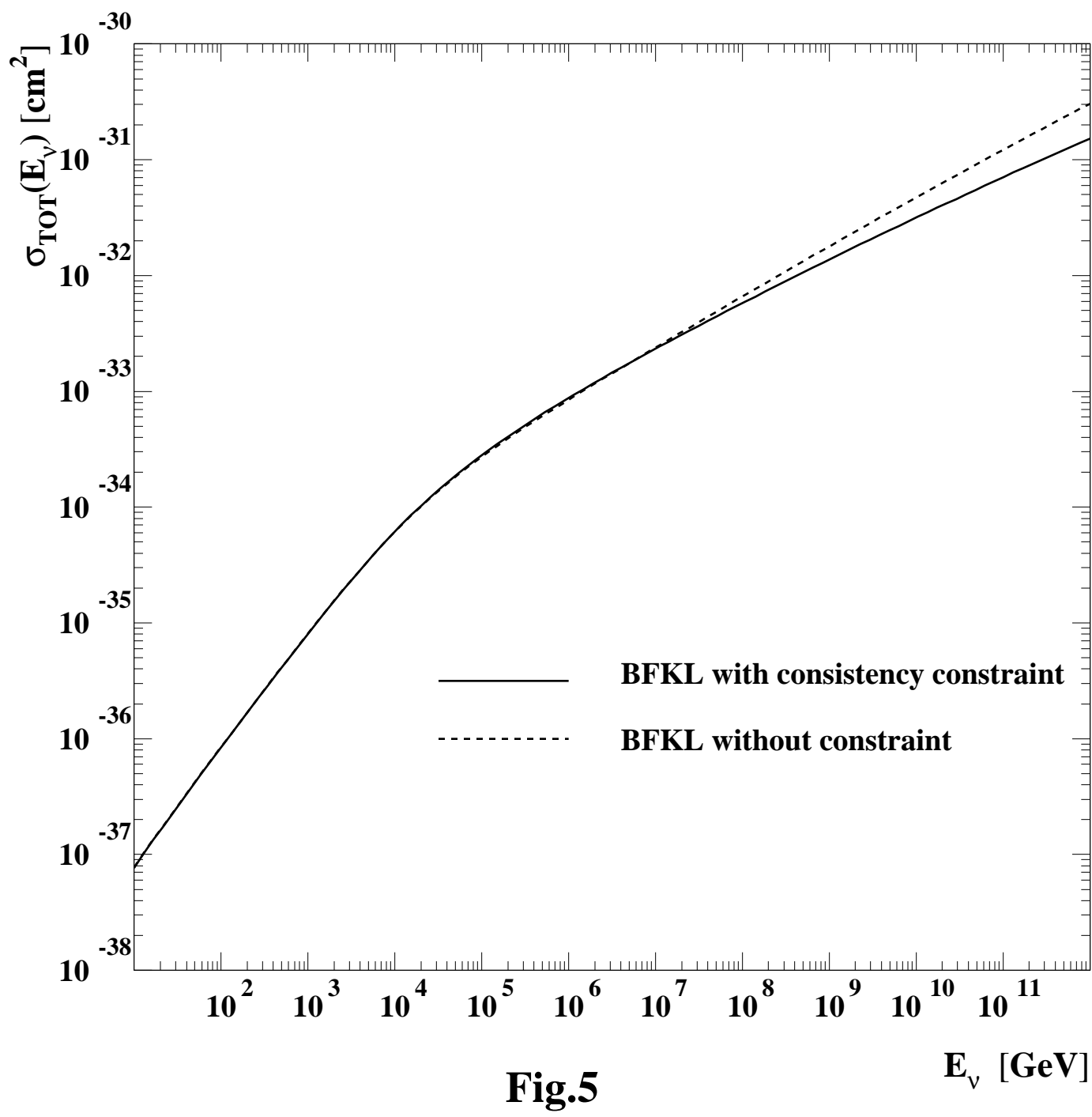


Fig.4

E_v [GeV]



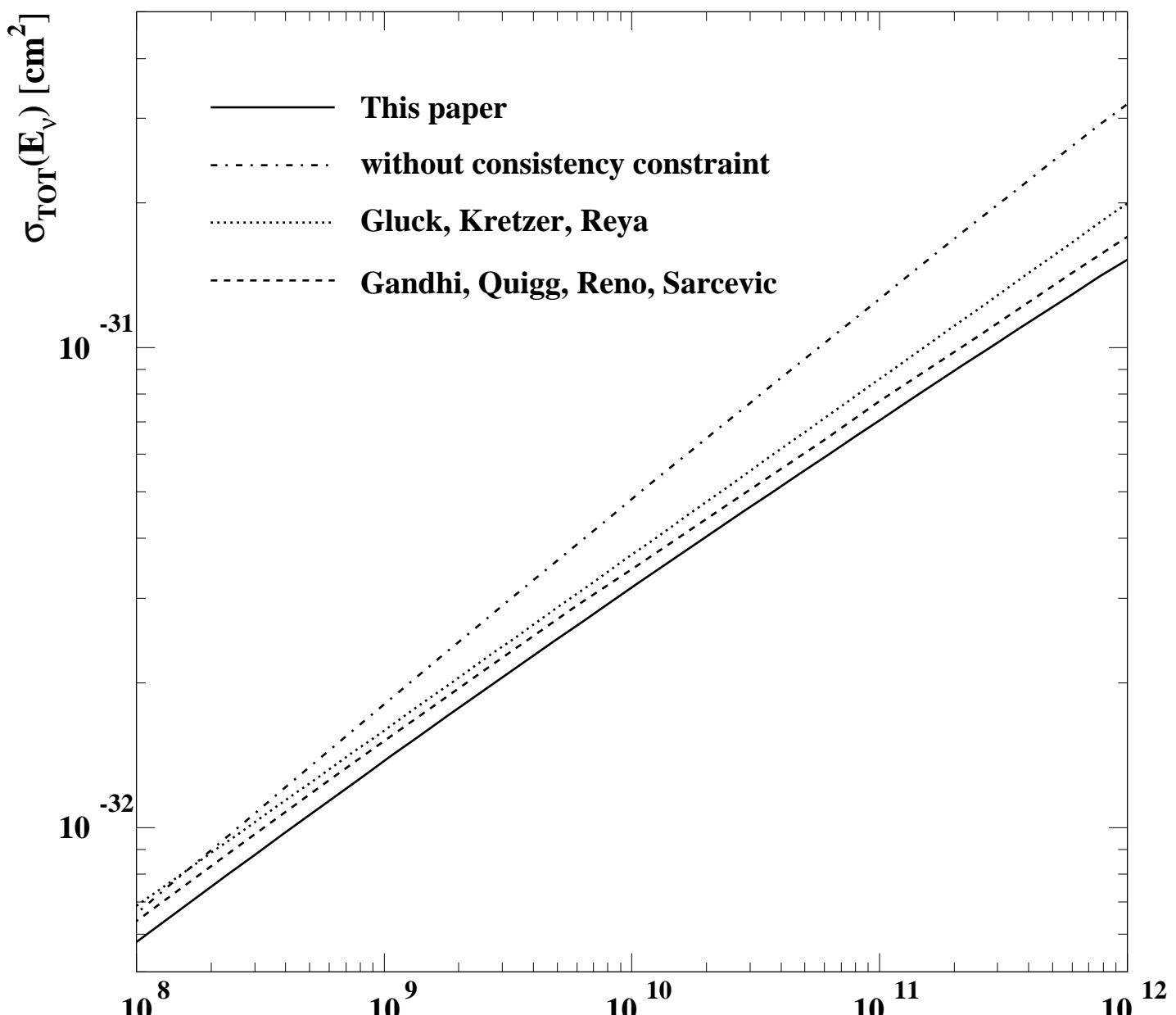


Fig.6

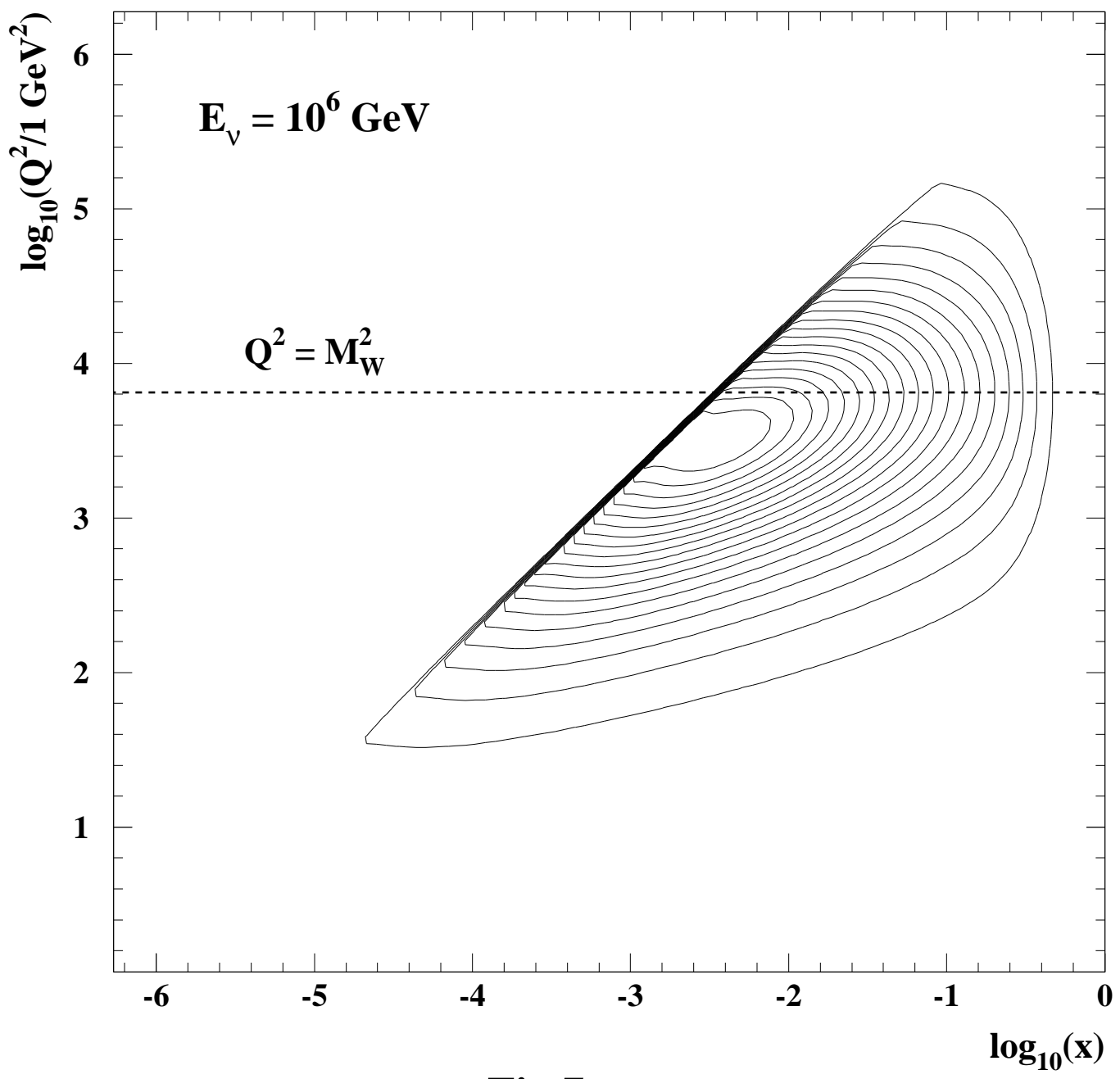


Fig.7a

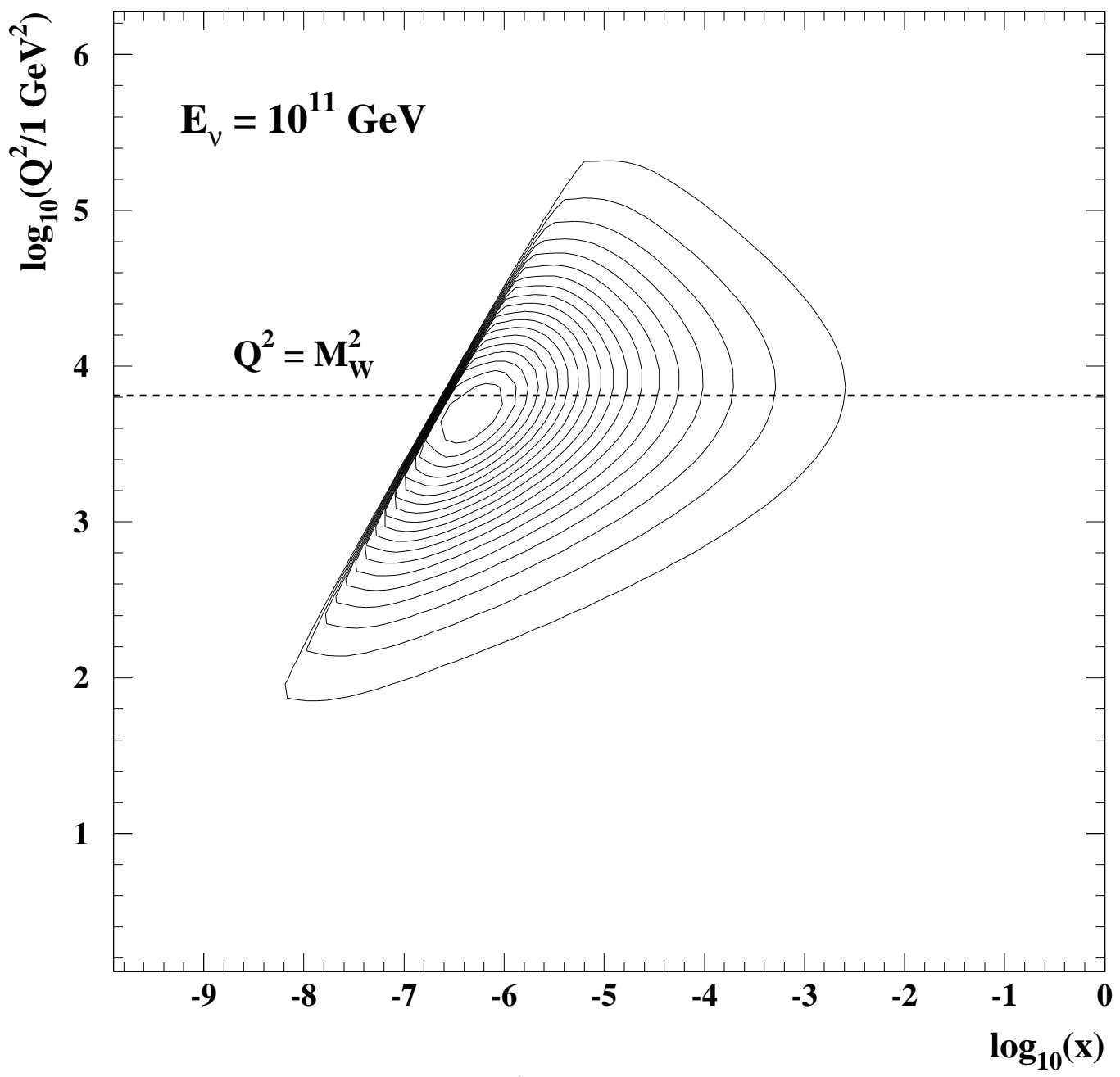
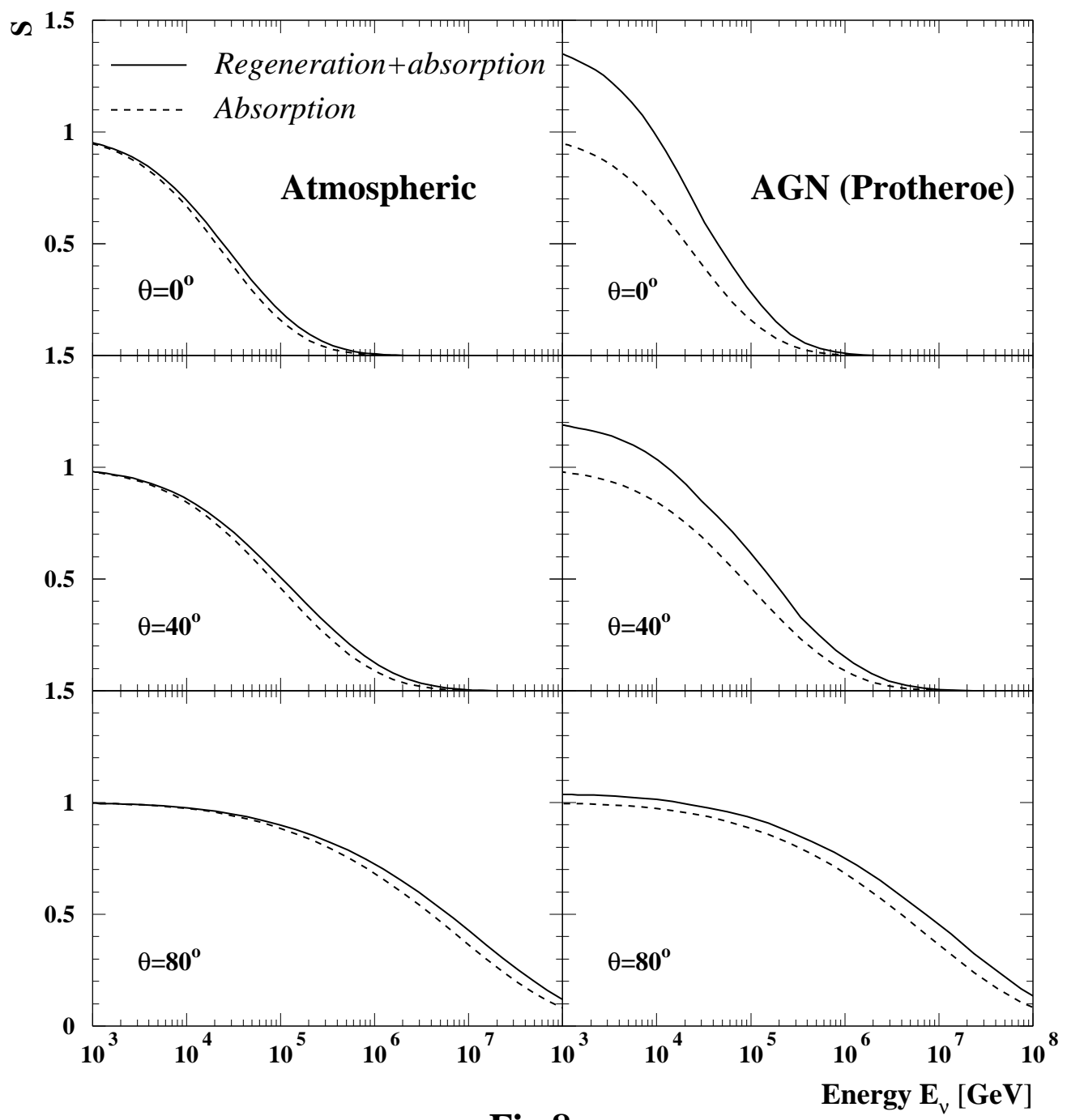


Fig.7b



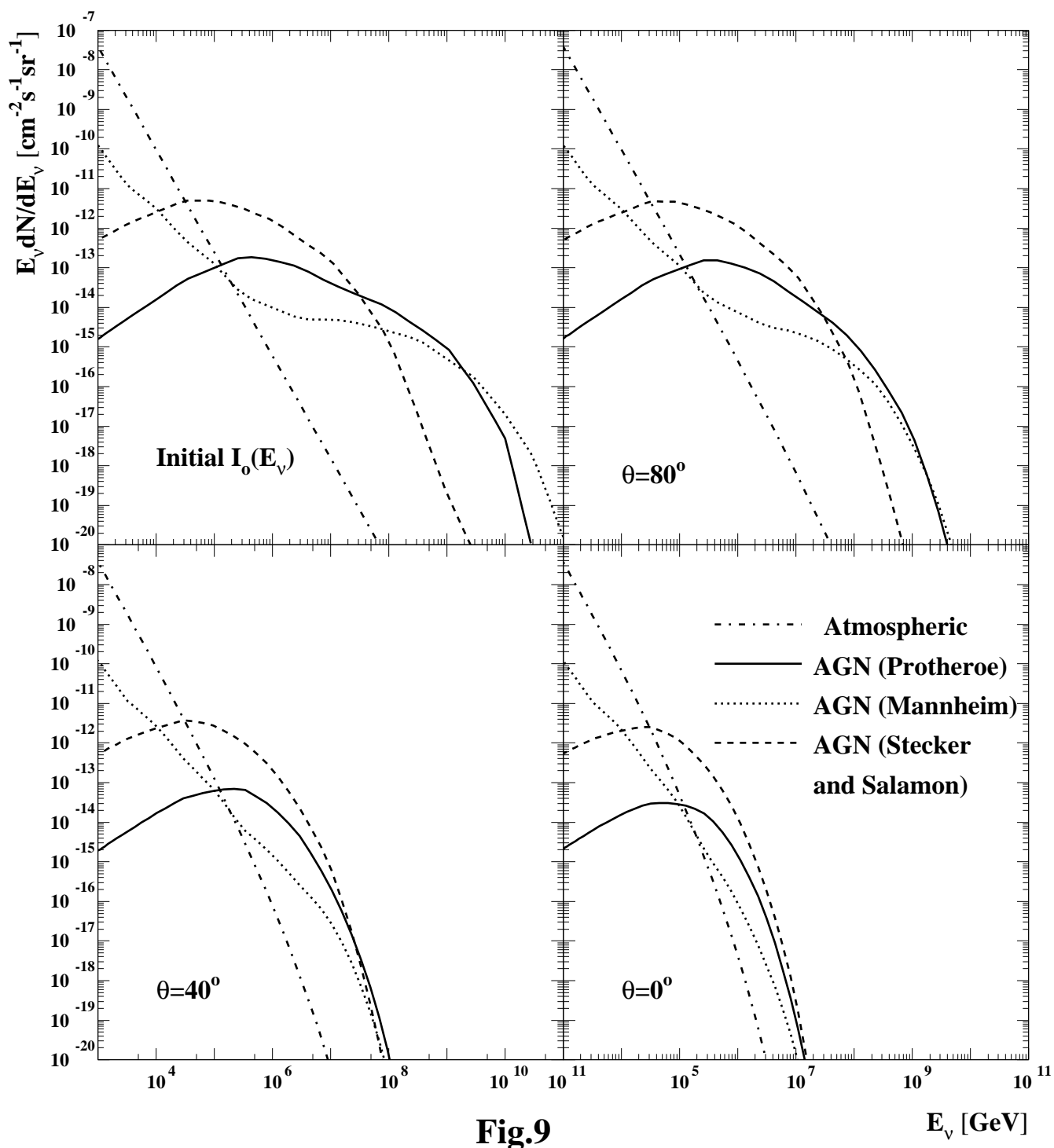


Fig.9

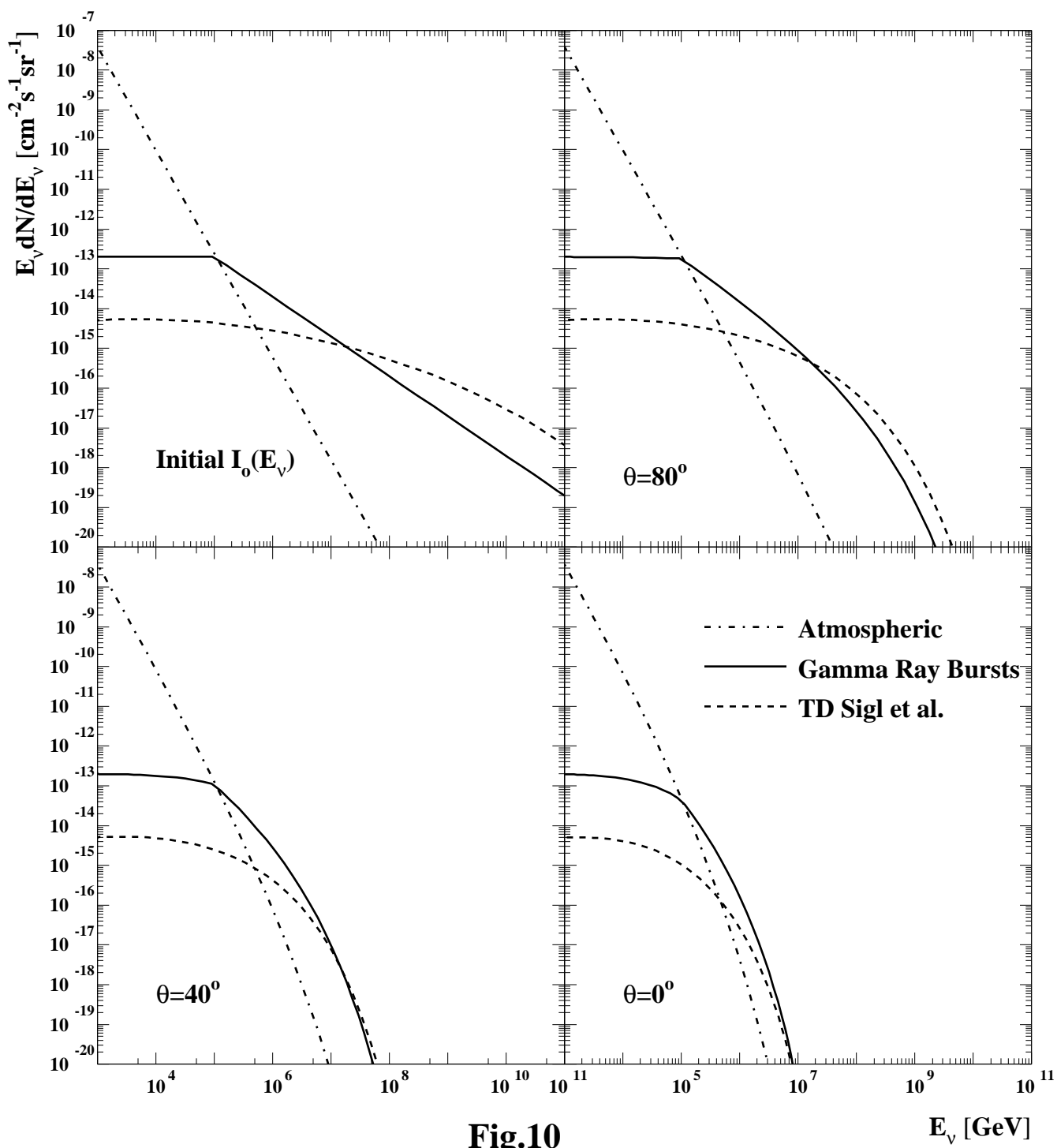


Fig.10